Advances in Science and Technology Research Journal

Advances in Science and Technology Research Journal, 2026, 20(7), 308–324
https://doi.org/10.12913/22998624/219866
ISSN 2299-8624, License CC-BY 4.0

Received: 2026.02.20
Accepted: 2026.05.15
Published: 2026.06.01

Second-order dynamic analysis of semi-rigid steel frames via a novel finite element method with consistent mass matrices

Quoc Anh Vu[1], Dung Bao Trung Le[1], Hai Quang Nguyen[2*]

[1] Faculty of Civil Engineering, Hanoi Architectural University, Hanoi, Vietnam
[2] Faculty of Mechanical-Automotive and Civil Engineering, Electric Power University, Hanoi, Vietnam
* Corresponding author's e-mail: quangnh@epu.edu.vn

ABSTRACT

In practical analysis, steel frames are often idealized with fully rigid or hinged connections, although actual connections exhibit semi-rigid behavior that can be modeled as rotational springs. Existing literature predominantly addresses static performance, whereas comprehensive studies dealing with geometrically nonlinear dynamic behavior of semi-rigid steel frames are still relatively scarce. This paper therefore proposes a new consistent mass matrix and an effective displacement-based finite element formulation for analyzing semi-rigid steel frames under dynamic loads, including P-Delta effects. A new expression for determining the reversal moment under dynamic loading is also introduced. The proposed algorithm fully represents the nonlinear hysteretic response of semi-rigid connections, enabling computation of frame's nonlinear dynamic response. A MATLAB program was developed and validated against published results. The analyses show that connection hysteresis and geometric nonlinearity significantly affect the transient response of steel frames.

Keywords: semi-rigid connection, P-Delta effect, consistent mass matrix, dynamic loads, nonlinear transient response.

INTRODUCTION

Steel frame structures are widely used in high-rise buildings. For simplicity, beam-column connections are often idealized as fully rigid or hinged. In reality, however, these connections deform and exhibit intermediate stiffness, which may lead to inaccurate predictions of structural response. Therefore, more reliable analysis methods should explicitly account for semi-rigid connection behavior. Previous studies [1–5] have shown that semi-rigid connections significantly influence frame performance. Because steel frames consist of slender members, P-Delta effects are also important and should be considered. Although these issues are recognized in design standards such as American steel structure design standards [6] and European steel structure design standards [7], specific computational procedures for analyzing semi-rigid steel frames including P-Delta effects are not fully developed in these standards.

For complex structural configurations such as semi-rigid steel frames, obtaining exact analytical solutions for dynamic behavior is inherently challenging. Consequently, most studies rely on numerical methods, particularly the finite element method (FEM). Therefore, developing an effective finite element formulation that incorporates both dynamic loading and P–Delta effects is essential. General procedures for constructing linear elastic and geometric stiffness matrices in evaluating the second-order static behavior of steel frames with semi-rigid connections under P-Delta actions were presented in [8]. For accurate dynamic analysis, however, a consistent mass matrix must be derived in addition to these stiffness matrices and the conventional lumped mass matrix. This mass matrix should vary with the instantaneous rotational stiffness at beam ends, which depends on the evolving geometric configuration. Hence, dynamic analysis of semi-rigid steel frames fundamentally depends on appropriate stiffness and mass formulations.

Chan and Ho (1994) [9] idealized the rotational flexibility of the joint as an independent spring element and combined it with a beam element possessing fully rigid end connections to establish a hybrid beam-column formulation. In this configuration, the stiffness of the hybrid element was obtained by embedding the joint stiffness into the bending components of the conventional elastic beam matrix. Based on this approach, Batelo et al. (2015) [10] developed a dynamic analysis method that considers geometric nonlinearity; however, the procedure for constructing the mass matrix was not clearly described.

Chen and Lui (1987) [2] modified beam-end rotations in the slope-deflection formulation using stability functions to construct stiffness matrices for beam-column elements with semi-rigid ends. The extension of this formulation to dynamic applications was later undertaken by Lui and Lopes (1997) [11] and Awkar and Lui (1999) [12], who adopted bilinear connection models together with a constant mass matrix assumption. Nguyen and Kim [13–15] analyzed elastic, inelastic, and spread-of-plasticity dynamics for semi-rigid steel frames, although the mass matrix formulation was not explicitly detailed. The P-Delta effect was considered in [11–15].

Nguyen (2012) [4] modified beam-end rotations by employing third-order Hermitian polynomials to interpolate the horizontal displacement, thereby deriving the linear elastic stiffness and consistent mass matrices for beam elements with semi-rigid ends. These formulations were subsequently applied to dynamic analysis using an elastic-plastic model; however, P-Delta effects were not included.

Chan and Ho (1994) [16] and Chan and Chui (2000) [5] established displacement functions and derived linear elastic stiffness, geometric stiffness, and consistent mass matrices for semi-rigid beam-column elements. Later studies [17] extended these formulations to second-order dynamic analysis of planar steel frames. Suarez et al. (1996) [18] and subsequent researchers [19, 20] derived consistent mass matrices considering eccentric connections and damping effects, though P-Delta effects were not fully incorporated in some cases. Zlatkov and co-authors [21–23] proposed alternative shape-function-based formulations and established consistent mass matrices for structures with semi-rigid connections.

Despite the significant contributions of the aforementioned studies, comprehensive investigations into the second-order dynamic behavior of semi-rigid steel frames remain relatively limited, particularly when both geometric nonlinearity and inertia effects are considered. Recent studies have further explored nonlinear modeling and dynamic response of semi-rigid steel frames [24–28]. In dynamic finite element analysis, inertia effects may be represented either by lumped mass matrices or by consistent mass matrices. While the lumped mass matrix is often adopted for computational simplicity, the consistent mass matrix generally provides improved accuracy in representing the distributed inertia of beam elements [29, 30]. Therefore, deriving a consistent mass matrix based on appropriate shape functions for beam elements with semi-rigid end connections is essential for reliable dynamic analysis.

To address these limitations, this study proposes a finite element formulation for the second-order dynamic analysis of semi-rigid steel frames based on a consistent mass matrix derived from newly developed displacement shape functions for beam–column elements with semi-rigid end connections. These shape functions, together with the corresponding stiffness matrices, were previously verified in static stability analysis [31] and provide a coherent framework for dynamic analysis. The proposed mass matrix consists of polynomial coefficients directly expressed in terms of instantaneous connection stiffness and element properties, ensuring computational simplicity. Limiting cases, including fully rigid and hinged connections, are also examined to verify the formulation.

Recent studies have made significant contributions to the development of finite element formulations for steel frames with semi-rigid connections. For example, Özel et al. [32] developed consistent matrices that account for shear deformation and rotary inertia effects, providing improved accuracy in structural modeling. In addition, Nguyen and Vu [33] proposed a condensed finite element formulation for semi-rigid steel frames, improving computational efficiency while maintaining acceptable accuracy.

Despite these valuable contributions, existing studies still treat key aspects of the problem separately. In particular, the combined effects of (i) consistent mass matrix formulation explicitly dependent on instantaneous connection stiffness, (ii) second-order (P–Δ) effects, and (iii) nonlinear hysteretic behavior of semi-rigid connections in dynamic

analysis have not been simultaneously incorporated within a unified finite element framework.

Therefore, the present study is the first to develop a unified formulation that integrates all these aspects into a single computational framework, enabling a more realistic and comprehensive representation of the dynamic response of semi-rigid steel frames.

The main contributions of this study can be summarized as follows:

1) A consistent mass matrix formulation is developed for beam–column elements with semi-rigid end connections based on newly established displacement shape functions.
2) A numerical framework is proposed for second-order dynamic analysis of steel frames considering both P–Delta effects and nonlinear semi-rigid connection behavior.
3) An efficient criterion is introduced to identify loading and unloading phases of semi-rigid connections during dynamic response analysis.
4) The effectiveness of the proposed formulation is verified through numerical examples and comparison with previously published results.

To overcome these limitations, the present study proposes a novel finite element formulation for the second-order dynamic analysis of semi-rigid steel frames using a consistent mass matrix. Unlike previous approaches, the proposed formulation explicitly incorporates a stiffness-dependent mass matrix together with geometric nonlinearity (P–Δ effects) and nonlinear hysteretic behavior of semi-rigid connections within a unified framework.

The remainder of this paper is organized as follows. First, the formulation of the element mass matrix is presented. Next, the modeling of semi-rigid connections under static and dynamic loading is described. The numerical procedure for second-order dynamic analysis is then introduced.

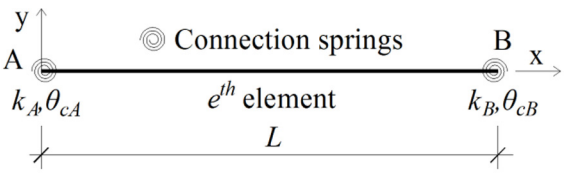

Figure 1. Hybrid element model

Finally, numerical verification and discussion are presented, followed by the conclusions.

FORMULATION OF THE ELEMENT MASS MATRIX

The purpose of the present formulation is to develop a consistent mass matrix and a computational procedure suitable for second-order dynamic analysis of steel frames with semi-rigid connections. The proposed methodology combines the displacement-based finite element formulation with a nonlinear connection model and an incremental time-integration scheme. The scope of the study focuses on planar steel frames subjected to dynamic loading while considering geometric nonlinearity and connection hysteresis. In the present formulation, the rotational flexibility of semi-rigid joints is represented by discrete rotational springs located at the ends of the beam-column element, resulting in a hybrid element e^{th} configuration as illustrated in Figure 1. This multi-spring element is characterized by two end nodes, A and B. The instantaneous rotational stiffness values at these ends are denoted by k_A and k_B, with corresponding rotation angles θ_{cA} and θ_{cB}. The springs are assumed to be dimensionless. Let L represent the element length. The kinematic assumptions and fundamental quantities adopted herein follow those described in [8]. The shape functions matrix for at these ends are denoted by and an element with semi-rigid end connections takes the following form:

$$\left[N(x)\right]=\begin{bmatrix} N_1(x) & 0 & 0 & N_4(x) & 0 & 0 \\ 0 & N_2(x) & N_3(x) & 0 & N_5(x) & N_6(x) \end{bmatrix} \tag{1}$$

where the shape functions are defined as follows

$$N_1(x)=1-\frac{x}{L},\quad N_2(x)=1-d_1x-3d_2x^2+d_3x^3,\quad N_3(x)=d_4x-d_5x^2+d_2x^3,$$

$$N_4(x)=\frac{x}{L},\quad N_5(x)=d_1x+3d_2x^2-d_3x^3,\quad N_6(x)=-d_6x-d_7x^2+d_8x^3 \tag{2}$$

Reference [8] provides the explicit expressions for coefficients from d_1 to d_8. To achieve reliable dynamic analysis of frame structures, a consistent mass formulation is adopted. When semi-rigid end connections are considered, the element mass matrix must account for the rotational degrees of freedom associated with these joints. Following the approaches in [5], [16], [34], the consistent mass matrix of the semi-rigid beam-column element, denoted as $[m_s]_e$, is derived by integrating the displacement interpolation functions over the element length, with m representing the mass per unit length of the member:

$$\left[m_s\right]_e = m\int_0^L \left[N(x)\right]^T \left[N(x)\right] dx \tag{3}$$

The coefficients of the matrix in Equation 3 are rewritten in the form:

$$\left[m_s\right]_e = q\begin{bmatrix} m_s^{1,1} & 0 & 0 & m_s^{1,4} & 0 & 0 \\ 0 & m_s^{2,2} & m_s^{2,3} & 0 & m_s^{2,5} & m_s^{2,6} \\ 0 & m_s^{3,2} & m_s^{3,3} & 0 & m_s^{3,5} & m_s^{3,6} \\ m_s^{4,1} & 0 & 0 & m_s^{4,4} & 0 & 0 \\ 0 & m_s^{5,2} & m_s^{5,3} & 0 & m_s^{5,5} & m_s^{5,6} \\ 0 & m_s^{6,2} & m_s^{6,3} & 0 & m_s^{6,5} & m_s^{6,6} \end{bmatrix} \tag{4}$$

Substituting the shape functions from Equation 2 into Equation 3 yields the coefficients of the consistent mass matrix. For brevity, the detailed polynomial expressions are not repeated here and can be found in [8]. The resulting coefficients are summarized in Equation 5.

$$m_s^{1,1} = m_s^{4,4} = \frac{L}{3},\ m_s^{1,4} = m_s^{4,1} = \frac{L}{6},$$

$$m_s^{2,2} = \frac{d_3^2 L^7}{7} - d_2 d_3 L^6 + \frac{\left(9d_2^2 - 2d_1 d_3\right)L^5}{5} + \frac{\left(6d_1 d_2 + 2d_3\right)L^4}{4} + \frac{\left(d_1^2 - 6d_2\right)L^3}{3} - d_1 L^2 + L,$$

$$m_s^{2,3} = m_s^{3,2} = \frac{d_2 d_3 L^7}{7} - \frac{\left(3d_2^2 + d_3 d_5\right)L^6}{6} + \frac{\left(-d_1 d_2 + 3d_2 d_5 + d_3 d_4\right)L^5}{5}$$
$$+ \frac{\left(d_1 d_5 - 3d_2 d_4 + d_2\right)L^4}{4} - \frac{\left(d_1 d_4 + d_5\right)L^3}{3} + \frac{d_4 L^2}{2}$$

$$m_s^{2,5} = m_s^{5,2} = -\frac{d_3^2 L^7}{7} + d_2 d_3 L^6 + \frac{\left(2d_1 d_3 - 9d_2^2\right)L^5}{5} - \frac{\left(6d_1 d_2 + d_3\right)L^4}{4} + \frac{\left(-d_1^2 + 3d_2\right)L^3}{3} + \frac{d_1 L^2}{2}$$

$$m_s^{2,6} = m_s^{6,2} = \frac{d_3 d_8 L^7}{7} - \frac{\left(3d_2 d_8 + d_3 d_7\right)L^6}{6} + \frac{\left(-d_1 d_8 + 3d_2 d_7 - d_3 d_6\right)L^5}{5}$$
$$+ \frac{\left(d_1 d_7 + 3d_2 d_6 + d_8\right)L^4}{4} + \frac{\left(d_1 d_6 - d_7\right)L^3}{3} - \frac{d_6 L^2}{2}$$

$$m_s^{3,3} = \frac{d_2^2 L^7}{7} - \frac{d_2 d_5 L^6}{3} + \frac{\left(2d_2 d_4 + d_5^2\right)L^5}{5} - \frac{d_4 d_5 L^4}{2} + \frac{d_4^2 L^3}{3}$$

$$m_s^{3,5} = m_s^{5,3} =$$
$$-\frac{d_2 d_3 L^7}{7} + \frac{\left(3d_2^2 + d_3 d_5\right)L^6}{6} + \frac{\left(d_1 d_2 - 3d_2 d_5 - d_3 d_4\right)L^5}{5} + \frac{\left(-d_1 d_5 + 3d_2 d_4\right)L^4}{4} + \frac{d_1 d_4 L^3}{3}$$

$$m_s^{3,6} = m_s^{6,3} =$$
$$\frac{d_2 d_8 L^7}{7} - \frac{\left(d_2 d_7 + d_5 d_8\right)L^6}{6} + \frac{\left(-d_2 d_6 + d_4 d_8 + d_5 d_7\right)L^5}{5} + \frac{\left(-d_4 d_7 + d_5 d_6\right)L^4}{4} - \frac{d_4 d_6 L^3}{3}$$

$$m_s^{5,5} = \frac{d_3^2 L^7}{7} - d_2 d_3 L^6 + \frac{\left(-2d_1 d_3 + 9d_2^2\right)L^5}{5} + \frac{3d_1 d_2 L^4}{2} + \frac{d_1^2 L^3}{3}$$

$$m_s^{5,6} = m_s^{6,5} =$$
$$-\frac{d_3 d_8 L^7}{7} + \frac{\left(3d_2 d_8 + d_3 d_7\right)L^6}{6} + \frac{\left(d_1 d_8 - 3d_2 d_7 + d_3 d_6\right)L^5}{5} - \frac{\left(d_1 d_7 + 3d_2 d_6\right)L^4}{4} - \frac{d_1 d_6 L^3}{3}$$

$$m_s^{6,6} = \frac{d_8^2 L^7}{7} - \frac{d_7 d_8 L^6}{3} + \frac{\left(-2d_6 d_8 + d_7^2\right)L^5}{5} + \frac{d_6 d_7 L^4}{2} + \frac{d_6^2 L^3}{3} \tag{5}$$

Particular limiting configurations of the consistent mass matrix arise when the semi-rigid connection stiffness tends toward extreme values, corresponding either to hinged conditions or fully rigid restraints. Based on these limits, four representative boundary cases are examined: two ends fully rigid, two ends hinged, and the two mixed configurations in which one end is rigid while the other behaves as a hinge. The limiting values of the matrix coefficients defined in Equation 5 are evaluated accordingly, and the resulting expressions are summarized in Table 1.
The data in Table 1 can be compiled into matrices for each special case as follows:

Case 1. Fully rigid connections at both ends

$$\left[m_s\right]_e = q\begin{bmatrix} \frac{L}{3} & 0 & 0 & \frac{L}{6} & 0 & 0 \\ 0 & \frac{13L}{35} & \frac{11L^2}{210} & 0 & \frac{9}{70L} & -\frac{13L^2}{420} \\ 0 & \frac{11L^2}{210} & \frac{L^3}{105} & 0 & \frac{13L^2}{420} & -\frac{L^3}{140} \\ \frac{L}{6} & 0 & 0 & \frac{L}{3} & 0 & 0 \\ 0 & \frac{9}{70L} & \frac{13L^2}{420} & 0 & \frac{13L}{35} & -\frac{11L^2}{210} \\ 0 & -\frac{13L^2}{420} & -\frac{L^3}{140} & 0 & -\frac{11L^2}{210} & \frac{L^3}{105} \end{bmatrix} \tag{6}$$

Case 2. End A fully rigid and end B hinged

$$[m_s]_e = q\begin{bmatrix} \frac{L}{3} & 0 & 0 & \frac{L}{6} & 0 & 0 \\ 0 & \frac{17L}{35} & \frac{3L^2}{35} & 0 & \frac{39L}{280} & 0 \\ 0 & \frac{3L^2}{35} & \frac{2L^3}{105} & 0 & \frac{11L^2}{280} & 0 \\ \frac{L}{6} & 0 & 0 & \frac{L}{3} & 0 & 0 \\ 0 & \frac{39L}{280} & \frac{11L^2}{280} & 0 & \frac{33L}{140} & 0 \\ 0 & 0 & 0 & 0 & 0 & 0 \end{bmatrix} \tag{7}$$

Case 3. Hinged connection at end A and rigid connection at end B

$$[m_s]_e = q\begin{bmatrix} \frac{L}{3} & 0 & 0 & \frac{L}{6} & 0 & 0 \\ 0 & \frac{33L}{140} & 0 & 0 & \frac{39L}{280} & -\frac{11L^2}{280} \\ 0 & 0 & 0 & 0 & 0 & 0 \\ \frac{L}{6} & 0 & 0 & \frac{L}{3} & 0 & 0 \\ 0 & \frac{39L}{280} & 0 & 0 & \frac{17L}{35} & -\frac{3L^2}{35} \\ 0 & -\frac{11L^2}{280} & 0 & 0 & -\frac{3L^2}{35} & \frac{2L^3}{105} \end{bmatrix} \tag{8}$$

Case 4. Hinged connections at both ends

$$[m_s]_e = q\begin{bmatrix} \frac{L}{3} & 0 & 0 & \frac{L}{6} & 0 & 0 \\ 0 & \frac{L}{3} & 0 & 0 & \frac{L}{6} & 0 \\ 0 & 0 & 0 & 0 & 0 & 0 \\ \frac{L}{6} & 0 & 0 & \frac{L}{3} & 0 & 0 \\ 0 & \frac{L}{6} & 0 & 0 & \frac{L}{3} & 0 \\ 0 & 0 & 0 & 0 & 0 & 0 \end{bmatrix} \tag{9}$$

Table 1. Coefficient values of the consistent mass matrix for limiting boundary configurations

Matrix coefficient $[m_s]_e$	Two ends fully rigid $k_A \to \infty$, $k_B \to \infty$	End A fully rigid while end B hinged $k_A \to \infty$, $k_B \to 0$	End A hinged while end B fully rigid $k_A \to 0$, $k_B \to \infty$	Two ends hinged $k_A \to 0$, $k_B \to 0$
$m_s^{2,2}$	$\frac{13L}{35}$	$\frac{17L}{35}$	$\frac{33L}{140}$	$\frac{L}{3}$
$m_s^{2,3}$, $m_s^{3,2}$	$\frac{11L^2}{210}$	$\frac{3L^2}{35}$	0	0
$m_s^{2,5}$, $m_s^{5,2}$	$\frac{9L}{70}$	$\frac{39L}{280}$	$\frac{39L}{280}$	$\frac{L}{6}$
$m_s^{2,6}$, $m_s^{6,2}$	$-\frac{13L^2}{420}$	0	$-\frac{11L^2}{280}$	0
$m_s^{3,3}$	$\frac{L^3}{105}$	$\frac{2L^3}{105}$	0	0
$m_s^{3,5}$, $m_s^{5,3}$	$\frac{13L^2}{420}$	$\frac{11L^2}{280}$	0	0
$m_s^{3,6}$, $m_s^{6,3}$	$-\frac{L^3}{140}$	0	0	0
$m_s^{5,5}$	$\frac{13L}{35}$	$\frac{33L}{140}$	$\frac{17L}{35}$	$\frac{L}{3}$
$m_s^{5,6}$, $m_s^{6,5}$	$-\frac{11L^2}{210}$	0	$-\frac{3L^2}{35}$	0
$m_s^{6,6}$	$\frac{L^3}{105}$	0	$\frac{2L^3}{105}$	0

In the limiting case where both ends of the beam–column element are fully rigid, the consistent mass matrix reduces to the classical formulations reported by Przemieniecki (1968) [34], Kwon and Bang (2000) [35], and Chopra (2020) [29]. When both ends are hinged, the formulation degenerates to the conventional element mass matrix given in [34].

SEMI-RIGID CONNECTION MODELING

An accurate representation of semi-rigid connection behavior is crucial for dynamic analysis of steel frame systems. Experimental investigations reported in [5] indicate that semi-rigid connections exhibit stable and repeatable hysteretic responses under cyclic loading, with pronounced ductility in their moment–rotation $M - \theta_c$ characteristics. For practical dynamic simulations, the nonlinear moment–rotation relationship obtained from static monotonic tests may be employed within simplified computational schemes. In general, three principal approaches are available for modeling cyclic joint behavior: independent hardening formulations, kinematic hardening models, and bounding surface techniques [5]. The present work adopts the independent hardening method.

Semi-rigid connection model under static loading

The mechanical response of a semi-rigid connection is characterized by the instantaneous relationship between bending moment and rotation at the connection. When the connection stiffness remains constant, this relationship is linear. For connections exhibiting stiffness degradation, the moment–rotation behavior is commonly represented using empirical curve-fitting formulations derived from experimental observations [5]. These formulations constitute the mathematical models employed to describe semi-rigid joint behavior, with parameters calibrated from test data.

In contrast to the linear representation, nonlinear models capture the progressive reduction

of stiffness as the applied moment increases. Various nonlinear formulations have been proposed in the literature; the present study adopts the exponential model introduced by Chen and Lui (1986, 1988) [5, 17, 36, 37], widely known as the Chen–Lui model. This model has been widely adopted in previous studies to represent the nonlinear moment–rotation behavior of semi-rigid steel connections. It has also been experimentally validated for common steel beam–column connections such as flush end-plate and angle connections, which are similar to the types of connections considered in this study. The corresponding moment–rotation relationship is expressed as:

$$M = M_0 + \sum_{j=1}^{n} C_j \left[1 - \exp\left(\frac{-|\theta_c|}{2j\alpha}\right) \right] + k_p |\theta_c| \quad (10)$$

The associated tangent rotational stiffness k_c is obtained by differentiating Equation 10 with respect to the rotation angle:

$$k_c = \left.\frac{dM}{d\theta_c}\right|_{|\theta_c|=|\theta_c|} = \sum_{j=1}^{n} \frac{C_j}{2j\alpha} \exp\left(\frac{-|\theta_c|}{2j\alpha}\right) + k_p \quad (11)$$

The initial stiffness k_0 can be obtained as:

$$k_0 = \left.\frac{dM}{d\theta_c}\right|_{|\theta_c|=0} = \sum_{j=1}^{n} \frac{C_j}{2j\alpha} + k_p \quad (12)$$

Here, M_0 denotes the initial moment, k_p represents the strain-hardening stiffness, α is a scaling parameter, C_j corresponds to the curve-fitting coefficient, and n indicates the number of exponential terms considered in the formulation. The curve-fitting parameters for various connection configurations were calibrated by Lui and Chen (1988) [5], including single web angle, top-and-bottom seated angle, flush end plate, and extended end plate joints.

The symbol C_j used in the Chen–Lui formulation represents a curve-fitting coefficient of the moment–rotation model and should not be confused with the damping matrix $[C]$ appearing in the global dynamic equilibrium equation.

Semi-rigid connection model under dynamic loading

The present study uses the Independent Hardening Method to model the connection under dynamic loading. According to this method, the properties of the connections are considered to remain constant during loading and unloading. In contrast, potential degradation phenomena, including variations in initial stiffness and initial yield moment, are neglected. Moreover, because the each hysteretic cycle is treated independently, no cumulative hardening effects are introduced. The hysteretic moment–rotation response of the semi-rigid connection subjected to dynamic loading using the Independent Hardening Method is shown in Figure 2. Under dynamic load, the hysteresis loop and tangential stiffness of the connection change according to the instantaneous bending moment M, the relative rotation angle θ_c and the variation of the moment. The following section presents an algorithm for modeling the nonlinear response of semi-rigid connections during dynamic excitation. This algorithm is already available in many open documents; however, the distinguishing feature of this formulation is that the loading and unloading phases are determined based on the difference in the absolute values of the moment at two adjacent time steps. During forward time integration, this criterion effectively distinguishes loading from unloading in each hysteretic loop.

The fundamental moment–rotation $M - \theta_c$ relationship adopted from [5] is expressed as:

$$M = f(\theta_c) \quad (13)$$

where: M denotes the bending moment as a function of the rotation θ_c.

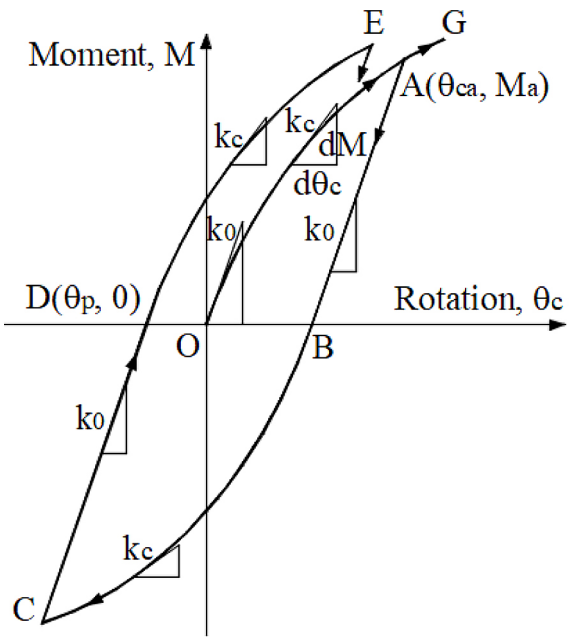

Figure 2. Connection behavior in the independent hardening method

When the response trajectory originates from or intersects the point (θ_p, 0). If the path starts from or passes through a point (θ_p, 0) located on the x-axis (M = 0) and subsequently proceeds along the primary branches (e.g., OA, BC, or DE), the connection is considered to be in the loading phase ($|M_{i+1}| - |M_i| > 0$, and follow the curve of the model with ($\theta_{p,}$ 0) serving as the updated reference configuration, where θ_p represents the last permanent connection rotation. $|M_i|$ and $|M_{i+1}|$ are the moments at the i^{th} and $(i + 1)^{th}$ time step, respectively. The $M - \theta_c$ relationship is then expressed by the following simple expression:

$$M = f\left(\theta_c - \theta_p\right) \tag{14}$$

The corresponding tangent stiffness is obtained as:

$$k_c = \left.\frac{dM}{d\theta_c}\right|_{|\theta_c|=|\theta_c-\theta_p|} \tag{15}$$

When the response enters the unloading phase ($|M_{i+1}| - |M_i| < 0$), and follows segments AB or CD, it will move towards the x-axis, along a linear path whose slope equals the initial stiffness k_0 of connection. The unloading process initiates at the reversal point (θ_{ca}, M_a). The $M - \theta_c$ relationship is expressed as:

$$M = M_a - k_0\left(\theta_{ca} - \theta_c\right) \tag{16}$$

and tangent connection stiffness is:

$$k_c = \frac{dM}{d\theta_c} = k_0 \tag{17}$$

where: the reversal moment M_a is evaluated as:

$$M_a = f\left(\theta_{ca} - \theta_p\right) \tag{18}$$

In the case of a connection during unloading, for example from A to B, but only going to F and then back to A, this path will follow a straight line parallel to the initial stiffness until it reaches the reversal moment M_a. Next, if the connection continues to be reloaded ($|M_{i+1}| - |M_i| > 0$, the response then returns along the primary loading branch AG, originating from the previously accumulated permanent rotation point (θ_p, 0). In the calculation process, upon completion of each unloading cycle, both the updated permanent rotation θ_p and the associated reversal moment M_a are recorded for subsequent time steps. Additionally, an adequately small time increment is required to ensure numerical accuracy. The loading or unloading phases of a hysteresis loop are depicted in Figure 2.

NUMERICAL FRAMEWORK FOR SECOND-ORDER DYNAMIC ANALYSIS

In dynamic analysis of building structures, steel frames are subjected to both static and dynamic loads. Static loads act throughout the service life of the structure, whereas dynamic loads occur over specific time intervals. To accurately capture load effects, static analysis is first performed, followed by dynamic analysis, and the results are combined to evaluate the overall response. In some cases, dynamic analysis is conducted separately to assess dynamic effects independently. The preliminary static analysis is performed only to establish the initial equilibrium configuration and internal force state of the structure. The subsequent dynamic analysis is then carried out using a nonlinear time-integration procedure, in which geometric nonlinearity and connection hysteresis are fully considered during the transient response.

The second-order static formulation accounting for P–Delta effects in semi-rigid steel frames has been detailed in [8], and the corresponding computational workflow is illustrated in Figure 3. Upon completion of the i^{th} load increment, the stiffness matrix, internal force vector, and geometric configuration associated with large displacements are updated before proceeding to the subsequent increment $(i + 1)^{th}$. The parameters n and Eps denote the total number of load increments and the prescribed tolerance for variations in axial force between successive calculation steps. Furthermore, N_0, N_1, and N_{max} refer to the axial force from the previous step, the axial force from the current step, and the maximum axial-force change among all elements after each increment, respectively.

The dynamic response of steel frames subjected to time-varying loads is evaluated within a finite element framework by discretizing the time domain into incremental steps. For geometrically nonlinear systems, the governing equilibrium equations are solved through incremental time-integration schemes for ordinary differential equations [29]. As discussed by Chan and Chui (2000) [5], in transient analysis the structural state at is computed from the previously established equilibrium configuration at time t. At the i^{th} increment, the incremental equilibrium equations governing the global multi-degree-of-freedom system may therefore be expressed as [5, 29, 30]:

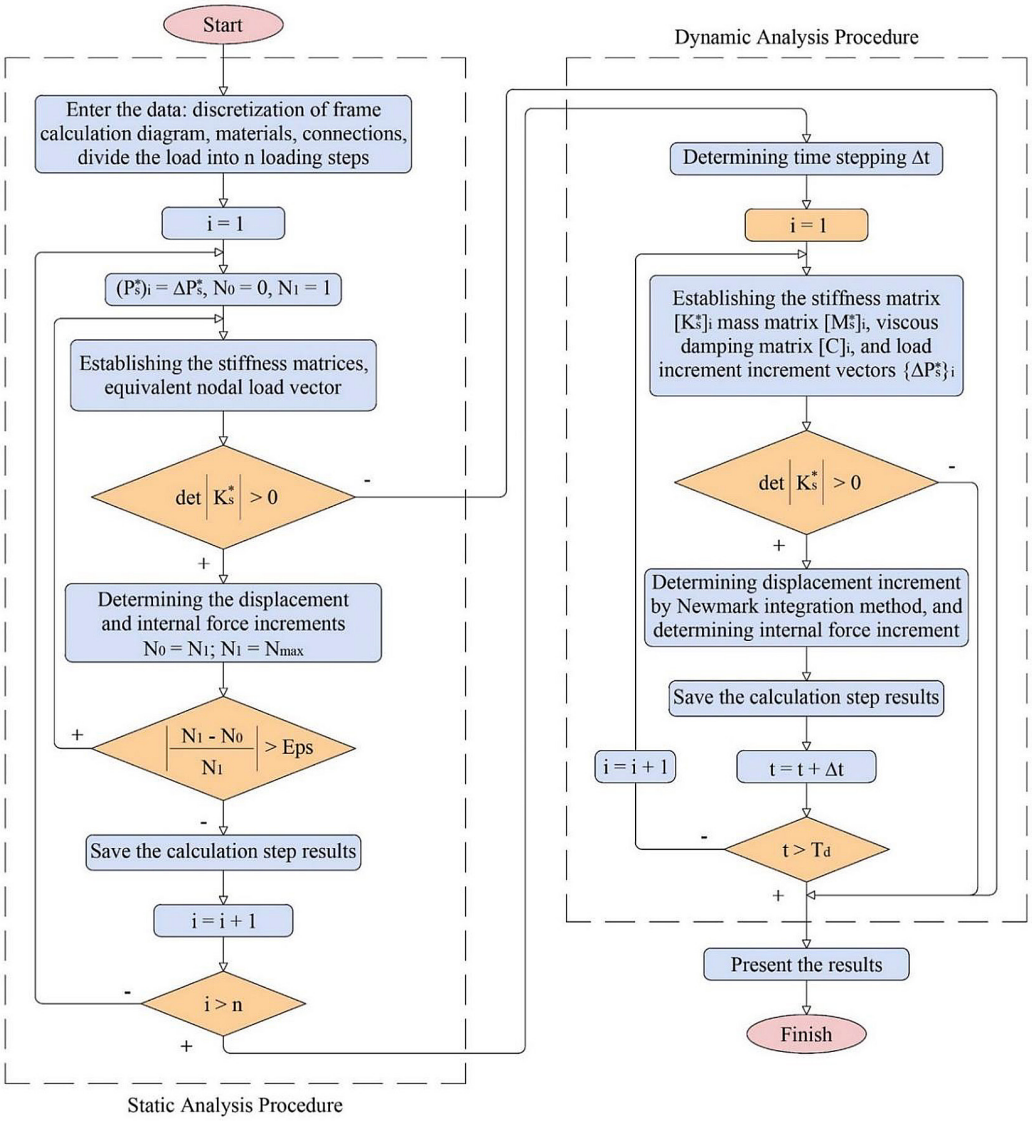

Figure 3. Numerical solution procedure for second-order dynamic analysis

$$\left[M_s^*\right]\left\{\Delta\ddot{\delta}_s^*\right\}+\left[C\right]\left\{\Delta\dot{\delta}_s^*\right\}+\left[K_s^*\right]\left\{\Delta\delta_s^*\right\}=\left\{\Delta P_s^*\right\} \quad (19)$$

where: $\left\{\Delta\ddot{\delta}_s^*\right\}$, $\left\{\Delta\dot{\delta}_s^*\right\}$, and $\left\{\Delta\delta_s^*\right\}$ denote the incremental acceleration, velocity, and displacement vectors, respectively. The matrix $\left[M_s^*\right]$ represents the mass matrix assembled from the consistent mass formulation in Equation 4 together with the lumped mass contribution. The viscous damping matrix $[C]$ is neglected in the present analysis. The stiffness matrix $\left[K_s^*\right]$ is formed from the linear elastic and geometric stiffness components given in [8], after imposing the relevant boundary conditions. The vector $\left\{\Delta P_s^*\right\}$ corresponds to the incremental applied nodal loads defined in [8].

Equation 19 is integrated in time using Newmark's scheme, a widely adopted direct time-integration approach [30]. The time increment Δt is selected to ensure sufficient accuracy, particularly with respect to the highest participating mode. In this study, the constant-average-acceleration variant of the Newmark method is employed, with parameters $\gamma=\frac{1}{2}$ and $\beta=\frac{1}{4}$

The total duration of the transient analysis is denoted by T_d. Accordingly, the number of time steps n_d is determined from Equation 20 as:

$$n_d=\frac{T_d}{\Delta t} \quad (20)$$

Step 1. Calculate the coefficients of the system of the equilibrium differential equations

At time step i, based on the updated connection stiffnesses, matrices $\left[K_s^*\right]_i$ and $\left[M_s^*\right]_i$ are calculated. The viscous damping matrix $\left[C\right]_i$ can be determined from damping models, but it is not considered in the present study. Calculate the dynamic load increment $\left[\Delta P_s^*\right]_i$.

At the first-time stepping $i = 1$, and at time $t = 0$, the initial conditions of dynamic analysis have the following form:

$$\left\{\delta_s^*\right\} = \left\{\delta_s^*\right\}_{(t=0)}, \quad \left\{\dot{\delta}_s^*\right\} = \left\{\dot{\delta}_s^*\right\}_{(t=0)},$$

$$\left\{\ddot{\delta}_s^*\right\} = \frac{\left\{P_s^*\right\}_{(t=0)} - \left[C\right]_{(t=0)}\left\{\dot{\delta}_s^*\right\}_{(t=0)} - \left[K_s^*\right]_{(t=0)}\left\{\delta_s^*\right\}_{(t=0)}}{\left[M_s^*\right]_{(t=0)}} \quad (21)$$

If the calculation model is subjected to static loads, the initial quantities in the dynamic analysis are inherited from the static analysis as shown in Equation 21. If the calculation model is not subjected to static loads, the initial stiffness of the connection is adopted.

Step 2. Establish the system of quasi-static equations

$$\left[\bar{K}_s^*\right]_i = \left[K_s^*\right]_i + \frac{\gamma}{\beta\Delta t}\left[C\right]_i + \frac{1}{\beta\left(\Delta t\right)^2}\left[M_s^*\right]_i \quad (22)$$

$$\left[a\right]_i = \frac{1}{\beta\Delta t}\left[M_s^*\right]_i + \frac{\gamma}{\beta}\left[C\right]_i \quad (23)$$

$$\left[b\right]_i = \frac{1}{2\beta}\left[M_s^*\right]_i + \Delta t\left(\frac{\gamma}{2\beta} - 1\right)\left[C\right]_i \quad (24)$$

$$\left\{\Delta\bar{P}_s^*\right\}_i = \left\{\Delta P_s^*\right\}_i + \left[a\right]_i\left\{\dot{\delta}_s^*\right\}_i + \left[b\right]_i\left\{\ddot{\delta}_s^*\right\}_i \quad (25)$$

Step 3. Determination of displacement, velocity, and acceleration at the current time increment

$$\left\{\Delta\delta_s^*\right\}_i = \left\{\Delta\bar{P}_s^*\right\}_i \Big/ \left[\bar{K}_s^*\right]_i \quad (26)$$

$$\left\{\Delta\dot{\delta}_s^*\right\} = \frac{\gamma}{\beta\Delta t}\left\{\Delta\delta_s^*\right\} - \frac{\gamma}{\beta}\left\{\dot{\delta}_s^*\right\} + \Delta t\left(1 - \frac{\gamma}{2\beta}\right)\left\{\ddot{\delta}_s^*\right\} \quad (27)$$

$$\left\{\Delta\ddot{\delta}_s^*\right\} = \frac{1}{\beta\left(\Delta t\right)^2}\left\{\Delta\delta_s^*\right\} - \frac{1}{\beta\Delta t}\left\{\dot{\delta}_s^*\right\} - \frac{1}{2\beta}\left\{\ddot{\delta}_s^*\right\} \quad (28)$$

Step 4. Evaluation of internal force increments

The displacement vector is first expressed in the global coordinate system, and the corresponding displacement increments are transformed to the local system. The internal force increments are then evaluated using the finite element formulation.

Step 5. Update of internal forces, displacements, and connection rotations

At the current time increment, internal forces, nodal displacements, and connection rotation angles are obtained by adding the computed increments to their respective values from the previous step.

Step 6. Update of connection stiffness and axial force

Based on the adopted semi-rigid joint model, which defines the moment–rotation relationship, both the bending moment and the associated rotation angle are updated. Using the structural displacements obtained in Step 5, the geometric configuration is revised, and the connection stiffness is recalculated for inclusion in the linear elastic, geometric stiffness, and mass matrices. Simultaneously, the axial force contribution in the geometric stiffness formulation is updated.

If the analysis time has not yet reached the prescribed final time, the procedure returns to Step 1. Otherwise, the computation terminates and the results are reported. The computational workflow is summarized in Figure 3.

NUMERICAL VERIFICATION AND DISCUSSION

Example 1 – Frame under cyclic loads, without gravity loads

This benchmark problem follows the configuration investigated by Chan and Chui (2000) [5] and later revisited by Silva et al. (2018) [17]. The example is used herein to assess the predictive capability of the proposed formulation by comparing the computed responses with previously published results.

The structure consists of an unbraced two-story planar steel frame subjected to horizontal cyclic loading at the floor levels. Gravity effects are excluded from the analysis. Beam members adopt the W360×72 section, while columns use W310×143 profiles in accordance with US standards. The Young's modulus is taken as 205 GPa. The numerical model, depicted in Figure 4, includes lumped masses of 3730 kg and 7460 kg. A triangular cyclic loading history ranging from −7.5 kN to +7.5 kN over a duration of 2 s is applied.

The column bases are hinged supports. Beam–column joints are modeled as flush end-plate connections, experimentally characterized

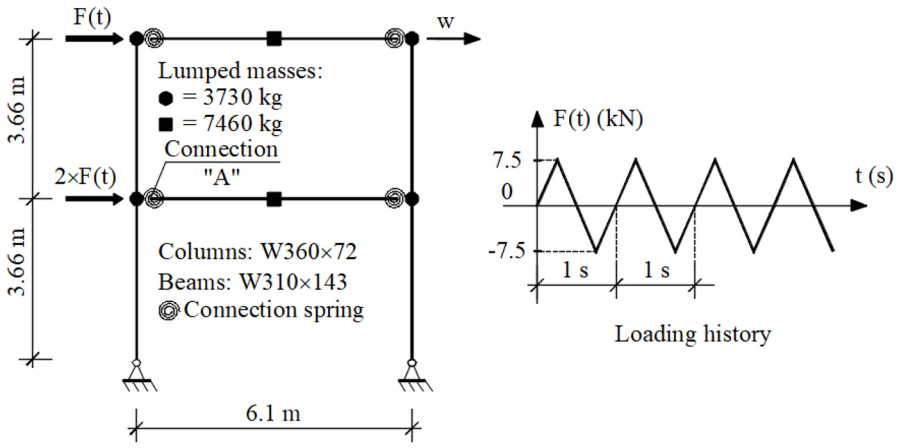

Figure 4. Model of frame under cyclic loads without gravity loads

by Ostrander [5] and represented using the Chen–Lui exponential formulation [17], with parameters: k_0 = 34804 kN · *m*/*rad*, M_0 = 0, k_p = 0.96415 × 10^3 kip · in / rad, α = 0.31783 × 10^{-3}, n = 6, C_1 = –0.25038 × 10^{-3}, C_2 = 0.50736 × 10^6, C_3 = -0.30396 × 10^5, C_4 = 0.75338 × 10^5, C_5 = -0.82873 × 10^5, C_6 = 0.33927 × 10^5.

The structural model represents the beam by two finite elements, whereas the column is modeled using a single element. Second-order effects due to P–Delta are incorporated in the analysis. The computed responses are presented in graphical form to facilitate comparison and validation. As illustrated in Figure 5, the time history of the top horizontal displacement under cyclic excitation is obtained. During the transient stage, the response varies between −7.4 cm and +7.4 cm; after approximately 6 s, it stabilizes and fluctuates around ±5.9 cm. At this stage, a balance is established between the externally supplied energy and the energy dissipated by the semi-rigid connections [17]. Although no explicit viscous damping matrix is included in the formulation, the nonlinear hysteretic behavior of the semi-rigid connections results in energy dissipation during cyclic deformation, which produces an apparent damping effect in the dynamic response.

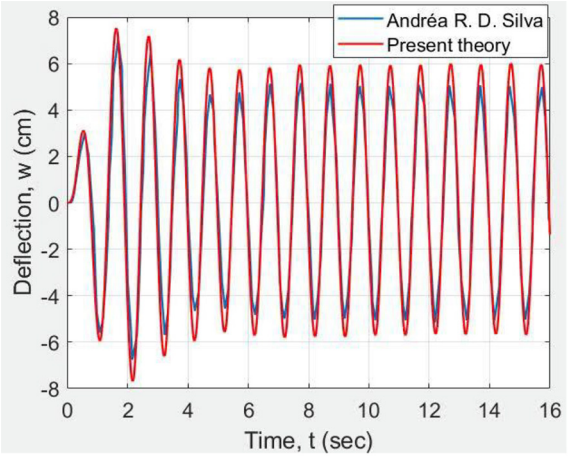

Figure 5. Time history of horizontal

The moment–rotation response of connection "A" is presented in Figure 6. The diagram $M - \theta_c$ shows that the hysteresis loops are highly reproducible and gradually stabilize after each oscillation period. The close agreement among the response curves confirms the robustness of the proposed dynamic analysis approach.

Example 2 – Frame subjected to rectangular impact loading considering gravity effects

Using the same steel frame as in Example 1, the authors in [5], [19], [38] studied the effects of the presence and absence of gravity loads when frames were subjected to rectangular impact loads.

This example uses the established second-order dynamics analysis method to study the same problem and verify the results with the studies mentioned. Static gravity loads of 36.6 kN are placed at the nodes, and 73.2 kN are placed between the beams. These loads increase the axial force and induce additional bending moments, thereby affecting the frame stiffness and the investigated displacement w. Rectangular impact loads, acting over 1 s, are applied to the pavement of the stories. The analytical model adopted for the frame is presented in Figure 7. The dynamic analysis starts from the initial equilibrium configuration with zero initial displacement and

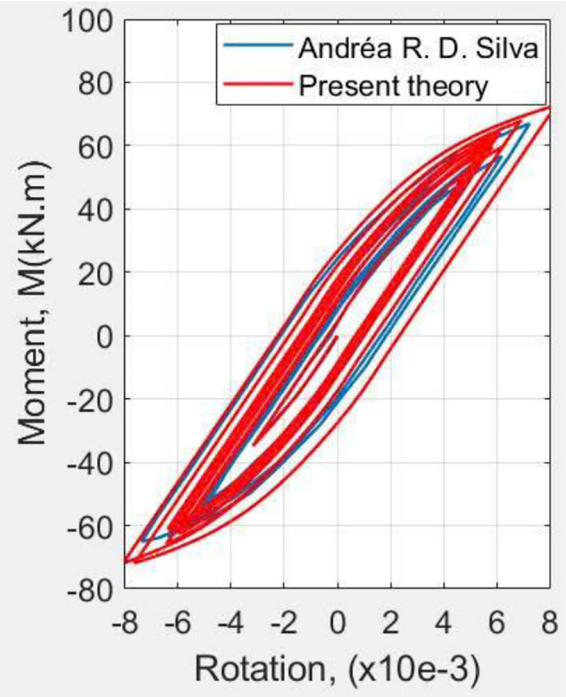

Figure 6. Moment–rotation relationship at connection "A"

velocity. In the analysis model, the beam is divided into two elements and the column into one element. Figure 8 presents the transient second-floor displacement analysis with and without gravity loads. The predicted results closely match those reported in [5], [19], [38], confirming the reliability of the proposed method. The frame with gravity loads exhibits larger deflection amplitudes due to stiffness reduction caused by the P-Delta effect. This behavior occurs because the presence of axial forces reduces the effective lateral stiffness of the frame, thereby amplifying the dynamic displacement response.

Although the initial structural system is symmetrical, permanent rotational deformations developing in the semi-rigid connections cause the displacement to gradually depart from the initial equilibrium position. The hysteresis damping induced in nonlinear semi-rigid connections also reduces the successive amplitude of the frame due to energy dissipation. Along with the above study and verification, this example also

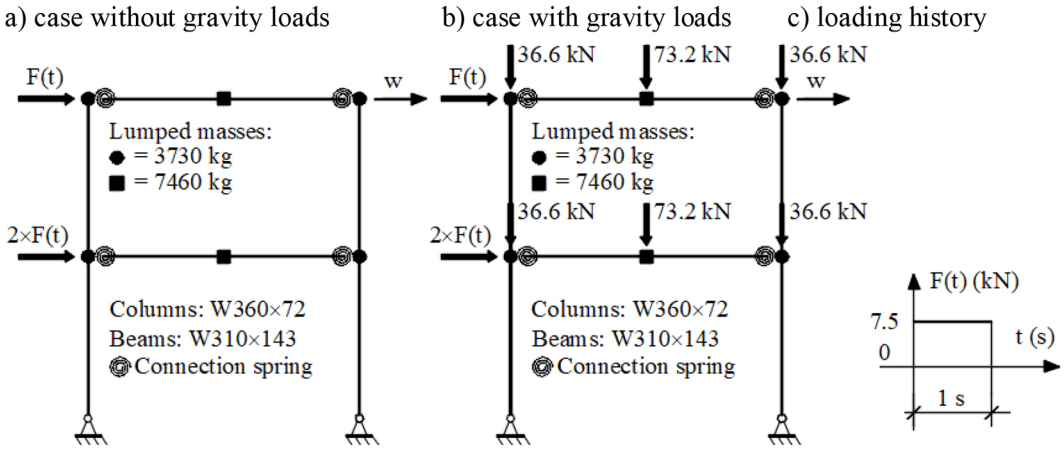

Figure 7. Steel frame subjected to rectangular impact loading

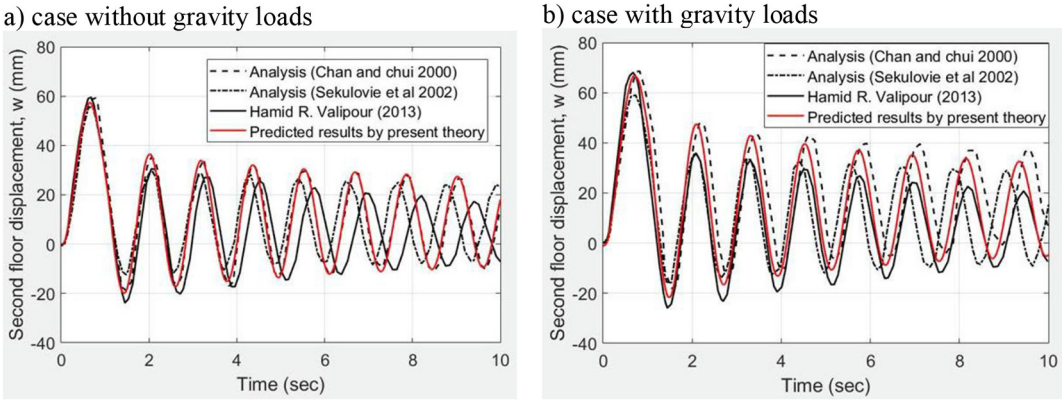

Figure 8. Transient displacement response of the frame

considers the effects of geometrically nonlinear computation cases, including $P - \delta$ (taking into account the effect of element deflection), $P - \Delta$ (taking into account the effects of displacement of frame nodes), and P-Delta (including $P - \delta$ and $P - \Delta$) on this steel frame.

With no gravity loads (as shown in Figure 9), or with gravity loads but small impact load values (as in Figures 10a-10c), the responses from the $P - \delta$ and P-Delta approaches are almost indistinguishable. The difference between the two nonlinear analysis methods becomes more pronounced as the impulse load increases, as shown in Figure 9 and Figure 10d. These figures also demonstrate that geometric nonlinear analysis yields more unfavorable results than those obtained without considering geometric nonlinearity.

Figure 11 shows that axial forces play a very important role in geometric nonlinear analysis methods. The correlation between the longitudinal force diagrams is highly consistent with the correlation between the displacement diagrams corresponding to the geometric nonlinear analysis methods. To simplify the calculation, if the frame has only a few stories and is subjected to small loads, it is sufficient to consider only the $P - \delta$ effect.

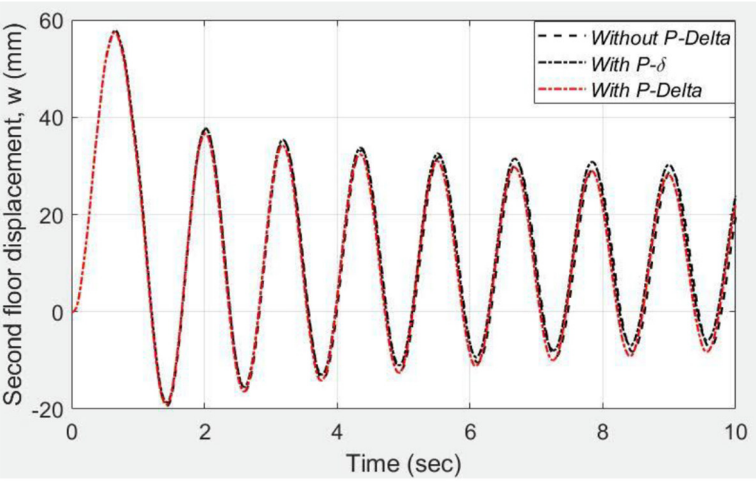

Figure 9. Comparison of geometric nonlinear effects without gravity loading

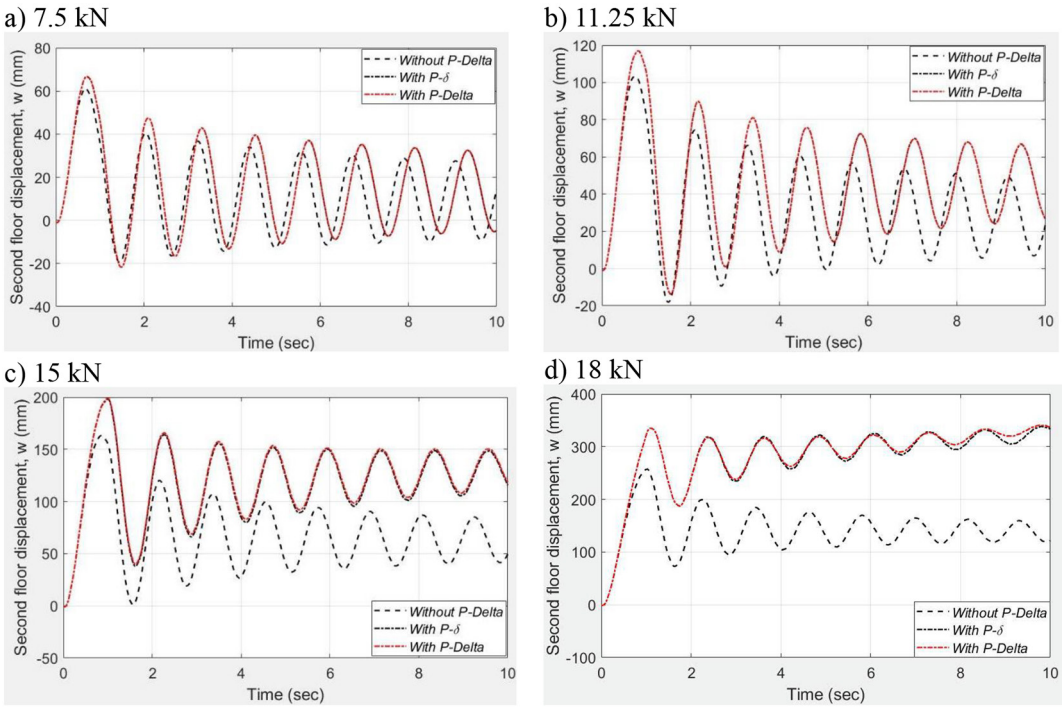

Figure 10. Influence of geometric nonlinear effects under gravity loading

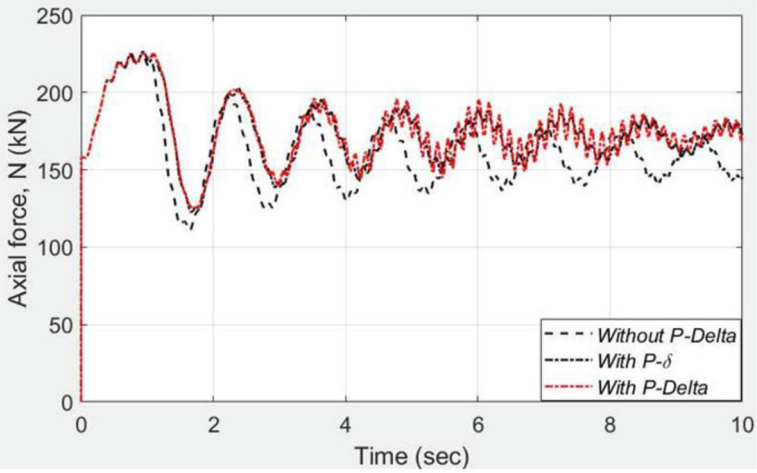

Figure 11. Axial force response under gravity and a rectangular impact load of 18 kN

CONCLUSIONS

In this study, semi-rigid beam–column connections are represented by rotational spring elements located at the member ends. A novel analytical approach is proposed to capture the realistic dynamic response of steel frames incorporating semi-rigid joints, explicitly accounting for geometric nonlinearity and connection characteristics. The formulation is based on a consistent mass matrix established simultaneously with the stiffness matrices and equivalent nodal load vectors derived from the corresponding shape functions. For static analysis, a combined incremental–iterative strategy is adopted, whereas the dynamic equilibrium equations are integrated using the Newmark time-stepping scheme. In addition, an efficient criterion is introduced to determine transition between loading and unloading phases over time.

Equation 5 demonstrates that the consistent mass matrix developed in this study for beam-column elements with semi-rigid end connections is both practical and effective for dynamic evaluation of steel frame systems with semi-rigid connections, which exhibit relatively complex behavior. This matrix consists entirely of polynomial coefficients, with parameters directly and simply expressed in terms of the instantaneous stiffness of the connections, together with the geometric characteristics and material parameters of the element. Equations 6–9 represent special cases of this consistent mass matrix, corresponding to situations where the connection stiffness at both ends approaches either infinity or zero. These cases are applicable to elements with fully rigid or fully pinned (hinged) ends. When semi-rigid connections are introduced at both member ends, the resulting hybrid element decreases the computational effort required for the analysis.

Numerical examples were conducted and validated against several related published studies. Although the results of the present study show minor deviations from previously published results, the predicted response curves remain highly consistent and closely aligned. The numerical results show good agreement with previously published studies, indicating that the proposed formulation is effective for analyzing the dynamic response of steel frames with semi-rigid connections considering P–Delta effects.

The numerical examples show that the hysteresis loops in nonlinear semi-rigid connections are highly reproducible and gradually stabilize after each oscillation cycle. Due to hysteresis damping in the connections, the steel frame gradually drifts from its initial equilibrium position, while the successive amplitudes decrease as a result of energy dissipation. Structural analysis of frames that include the P-Delta effect yields less favorable results than analyses that neglect it. When gravity and lateral loads are absent or small, the effects of geometric nonlinearity $P - \delta$ and the P-Delta effect are approximately equivalent. These two geometric nonlinear analysis approaches only diverge when the lateral load becomes significantly large. The present study also indicates that axial force has a pronounced effect on the frame's dynamic response. To simplify calculations, for low-rise frames subjected to small loads, this $P - \delta$ effect only needs to be considered. It should be noted that the present validation is based on two

representative numerical examples. Further studies involving larger structural systems and different types of semi-rigid connections may provide additional insights into the applicability of the proposed formulation.

The proposed formulation provides a practical framework for evaluating the dynamic behavior of steel frames with semi-rigid connections while accounting for geometric nonlinearity and connection hysteresis. From an engineering perspective, the method can support more realistic prediction of structural responses in steel frame systems subjected to dynamic loading.

Future studies may extend the proposed formulation to larger structural systems and different types of semi-rigid connections, as well as incorporate additional effects such as damping models and three-dimensional structural behavior. These developments may further facilitate the practical application of the proposed approach in advanced structural analysis and design.

REFERENCES

1. Stelmack T.W. Analytical and experimental response of flexibly-connected steel frames. Master Thesis. University of Colorado. Colorado, USA; 1980.
2. Chen W.F., Lui E.M. Structural Stability Theory and Implementation. Elsevier Science Publishing Co, Inc. New York, USA; 1987.
3. Anh V.Q., Leon R.T. Vibration analysis of steel frames with semi-rigid connections on an elastic foundation. Steel Compos. Struct. 2008; 8(4): 265–280. https://doi.org/10.12989/scs.2008.8.4.265
4. Quang N.H. Calculation of steel frames with semi-rigid connections according to the elastic-plastic model subjected to dynamic loads. Doctoral Thesis. Hanoi University of Architecture. Hà Nội, Việt Nam; 2012.
5. Chan S.L., Chui P.P.T. Non-linear static and cyclic analysis of steel frames with semi-rigid connections. Elsevier Science, Ltd. Oxford, UK; 2000.
6. AISC. LRFD Load and Resistance Factor Design Specification for Structural Steel Buildings. Chicago, Illinois, United States; 2000.
7. CEN. EN 1993-1-1 Design of steel structures. Part 1-1: General rules and rules for buildings. Brussels, Belgium; 2005.
8. Anh V.Q., Trung L.D.B., Quang N.H. Shape functions development for beam-column element with semi-rigid connections in second-order steel frame analysis. Civ. Eng. J. 2025; 11(1): 369–392. https://doi.org/10.28991/CEJ-2025-011-01-021
9. Chan S.L., Ho G.W.M. Nonlinear vibration analysis of steel frames with semirigid connections. J. Struct. Eng. 1994; 120(4): 1075–1087. https://doi.org/10.1061/(ASCE)0733-9445(1994)120:4(1075)
10. Batelo E.A.P., Silva A.R.D., Silveira R.A.M. Nonlinear transient analysis of steel frames structures with semi-rigid connections. In: The XXXVI Ibero-Latin American Congress on Computational Methods in Engineering (CILAMCE). Rio de Janeiro, Brazil; 2015. https://doi.org/10.20906/CPS/CILAMCE2015-0758
11. Lui E.M., Lopes A. Dynamic analysis and response of semirigid frames. Eng. Struct. 1997; 19(8): 644–654. https://doi.org/10.1016/S0141-0296(96)00143-5
12. Awkar J.C., Lui E.M. Seismic analysis and response of multistory semirigid frames. Eng. Struct. 1999; 21: 425–441. https://doi.org/10.1016/S0141-0296(97)00210-1
13. Nguyen P.C., Kim S.E. Nonlinear elastic dynamic analysis of space steel frames with semi-rigid connections. J. Constr. Steel Res. 2013; 84: 72–81. https://doi.org/10.1016/j.jcsr.2013.02.004
14. Nguyen P.C., Kim S.E. Nonlinear inelastic time-history analysis of three-dimensional semi-rigid steel frames. J. Constr. Steel Res. 2014; 101: 192–206. https://doi.org/10.1016/j.jcsr.2014.05.009
15. Nguyen P.C., Kim S.E. Second-order spread-of-plasticity approach for nonlinear time-history analysis of space semi-rigid steel frames. Finite Elem. Anal. Des. 2015; 105: 1–15. https://doi.org/10.1016/j.finel.2015.06.006
16. Chan S.L. Vibration and modal analysis of steel frames with semi-rigid connections. Eng. Struct. 1994; 16(1): 25–31. https://doi.org/10.1016/0141-0296(94)90101-5
17. Silva A.R.D., Batelo E.A.P., Silveira R.A.M., Neves F.A., Gonçalves P.B. On the nonlinear transient analysis of planar steel frames with semi-rigid connections: From fundamentals to algorithms and numerical studies. Lat. Am. J. Solids Struct. 2018; 15(3): 1–28. https://doi.org/10.1590/1679-78254087
18. Suarez L.E., Singh M.P., Matheu E.E. Seismic response of structural frameworks with flexible connections. Comput. Struct. 1996; 58(1): 27–41. https://doi.org/10.1016/0045-7949(95)00108-S
19. Sekulovic M., Salatic R., Nefovska M. Dynamic analysis of steel frames with flexible connections. Comput. Struct. 2002; 80: 935–955. https://doi.org/10.1016/S0045-7949(02)00058-5
20. Salatić R. Seismic analysis of steel frames with semi-rigid and viscous connections. Conference proceedings international conference. Subotica, Serbia; 2019: 87–98. https://doi.org/10.14415/konferencijagfs2019.008
21. Zlatkov D. Teorijska i eksperimentalna analiza armiranobetonskih linijskih nosača sa polukrutim vezama – theoretical and experimental analysis of reinforced concrete frame structures with semi-rigid

connections. Doctoral Thesis. Niš, Serbia; 2015.

22. Zlatkov D., Zdravkovic S., Mladenovic B., Stojic R. Matrix formulation of dynamic design of structures with semi-rigid connections. Facta Univ. Ser.: Archit. Civ. Eng. 2011; 9(1): 89–104. https://doi.org/10.2298/fuace1101089z
23. Zlatkov D., Zdravkovic S., Mladenovic B., Mijalkovic M. Seismic analysis of frames with semi-rigid connections in accordance with EC8. Facta Univ. Ser.: Archit. Civ. Eng. 2020; 18(2): 203–217. https://doi.org/10.2298/fuace201208015z
24. Genovese F, Sofi A. A novel interval matrix stiffness method for the analysis of steel frames with uncertain semi-rigid connections. Advances in Engineering Software. 2024;192:103629._https://doi.org/10.1016/j.advengsoft.2024.103629
25. Zhao H, Liu XG, Tao MX. Component-based model of semi-rigid connections for nonlinear analysis of composite structures. Engineering Structures. 2022;266:114542. https://doi.org/10.1016/j.engstruct.2022.114542
26. Zhao H, Qian XY, Liu XG, Chen HB, Tao MX. Dynamic responses of multi-story structural systems with separated gravity and lateral resisting systems under seismic action considering connection semi-rigidity effects. Engineering Structures. 2024;302:117386. https://doi.org/10.1016/j.engstruct.2023.117386
27. de Araújo FC, Ribeiro IS, Machado RM. Nonlinear analysis of semirigid steel frames having nonprismatic shear-deformable members. Engineering Structures. 2022;257:114047. https://doi.org/10.1016/j.engstruct.2022.114047
28. Lemes IJM, Silveira RAM, Teles LOM, Barros RC, Silva ARD. Numerical formulation for advanced non-linear static analysis of semi-rigid planar steel frames. Journal of the Brazilian Society of Mechanical Sciences and Engineering. 2023;45(7):428. https://doi.org/10.1007/s40430-023-04288-6
29. Chopra A.K. Dynamics of Structures Theory and Applications to Earthquake Engineering. Fifth Edit. Prentice-Hall International Series in Civil Engineering and Engineering Mechanics. UK; 2020.
30. Bathe K.J. Finite Element Procedures. Prentice-Hall, Inc. New Jersey, USA; 1996.
31. Anh V.Q., Quang N.H., Trung L.D.B. FEM-based prediction of elastic critical loads in steel frames with nonlinear semi-rigid connections. J. Mater. Constr. 2025; 15(1). https://doi.org/10.54772/jomc.v15i01.960
32. Özel H.F., Sarıtaş A., Taşbahji T. Consistent matrices for steel framed structures with semi-rigid connections accounting for shear deformation and rotary inertia effects. Engineering Structures. 2017; 137: 194–203
33. Nguyen T.D., Vu Q.A. Analysis of steel frame with semi-rigid connections and constraints using a condensed finite element formulation. International Journal of GEOMATE. 2023; 25(111): 113–121.
34. Przemieniecki J.S. Theory of matrix structural analysis. McGraw-Hill Book Company, Inc. New York, USA; 1968.
35. Kwon Y.W., Bang H. The Finite Element Method Using MATLAB. Second Edition. CRC Press LLC. Boca Raton, Florida, USA; 2000.
36. Chen W.F., Lui E.M. Stability Design of Steel Frames. Reissued. CRC Press. Boca Raton, Florida, USA; 2018. https://doi.org/10.1201/9781351076852
37. Nguyen P.C., Kim S.E. An advanced analysis method for three-dimensional steel frames with semi-rigid connections. Finite Elem. Anal. Des. 2014; 80: 23–32. https://doi.org/10.1016/j.finel.2013.11.004
38. Valipour H.R., Bradford M.A. Nonlinear P-Δ analysis of steel frames with semi-rigid connections. Steel Compos. Struct. 2013; 14(1): 1–20. https://doi.org/10.12989/scs.2013.14.1.001